Journal of Magnetism and Magnetic Materials 427 (2017) 220–224

Contents lists available at ScienceDirect

Journal of Magnetism and Magnetic Materials

journal homepage: www.elsevier.com/locate/jmmm

Surface functionalization of dopamine coated iron oxide nanoparticles for various surface functionalities

Jennifer Sherwood[a], Yaolin Xu[a], Kira Lovas[a], Ying Qin[b], Yuping Bao[a,*]

[a] Chemical and Biological Engineering, The University of Alabama, Tuscaloosa , AL 35487, USA
[b] Alabama Innovation and Mentoring of Entrepreneurs, The University of Alabama, Tuscaloosa, AL 35487, USA

ARTICLE INFO

Keywords:
Magnetic nanoparticles
Conjugation
Biomedical applications
Zwitterionic surface chemistries

ABSTRACT

We present effective conjugation of four small molecules (glutathione, cysteine, lysine, and *Tris*(hydroxymethyl) aminomethane) onto dopamine-coated iron oxide nanoparticles. Conjugation of these molecules could improve the surface functionality of nanoparticles for more neutral surface charge at physiological pH and potentially reduce non-specific adsorption of proteins to nanoparticles surfaces. The success of conjugation was evaluated with dynamic light scattering by measuring the surface charge changes and Fourier transform infrared spectroscopy for surface chemistry analysis. The stability of dopamine-coated nanoparticles and the ability of conjugated nanoparticles to reduce the formation of protein corona were evaluated by measuring the size and charge of the nanoparticles in biological medium. This facile conjugation method opens up possibilities for attaching various surface functionalities onto iron oxide nanoparticle surfaces for biomedical applications.

1. Introduction

Iron oxide nanoparticles (NPs) have been widely studied for biological and biomedical applications, including targeted drug delivery [1], cell tracking [2–5], and as magnetic resonance imaging (MRI) contrast agents [6–9]. For all these applications, surface functionalities of NPs are critical because they are the first encounter with biological systems. For instance, surfaces directly affect cellular uptake [10], biodistribution [11], blood circulation [12], toxicity [13], and metabolism [14]. Many of these biological behaviors can be attributed to the ability of NPs attracting native proteins, also known as protein corona, and subsequently intriguing immune responses [15,16]. Two effective surface coatings have been explored to overcome the surface effects, such as PEGylation [17] and the use of zwitterionic molecules [18]. The dense, hydrophilic layer of the polyethylene glycol (PEG) on NP surfaces minimizes NP aggregation under physiological conditions, and, additionally, the net neutral charge of the PEGylated NPs at physiological pH can reduce the formation of protein corona [19]. Alternatively, the neutrally charged surfaces of NPs coated with zwitterionic molecules is capable of repressing non-specific absorption of proteins onto NP surfaces [20]. Therefore, it is highly beneficial to have a functional NP surface, which allows for easy conjugation of various surface chemistries for desirable applications.

Several conjugation methods have been studied to link various molecules onto iron oxide NP surfaces, including proteins, PEG, and other small molecules [21–28]. The use of chemical linkers to cross-link NPs and molecules has been the most explored approach [29,30]. These linkers include carbodiimide (EDC) [31,32], N-hydroxylsuccinimide (NHS) ester cross-linker [33], and maleimide [34,35]. A general drawback for linker chemistry is the specific conjugation conditions and low conjugation efficiency, such as acidic conditions (pH 4.5–5.5) for EDC, pH 7.2–8.0 at 4 °C for NHS. The low conjugation efficiency is mainly a result of completion reactions. We recently showed that dopamine-functionalized surfaces of iron oxide NPs can easily conjugate with protein molecules [36,37], which also offers a great platform to link other molecules.

In this paper, we report the direct conjugation of various molecules onto dopamine-coated iron oxide NP surfaces *via* a facile, linker-free conjugation method previously developed by our group [38]. These small molecules include glutathione (GSH), cysteine (Cys), lysine (Lys), and tris(hydroxymethyl)aminomethane (Tris), which lead to various surface functionalities after conjugation. At physiological pH, these molecules are either zwitterionic ions or neutrally charged, which can potentially suppress the formation of the protein corona *in vitro* and *in vivo*. The success of conjugation was evaluated using Fourier transform infrared spectroscopy (FTIR). The hydrodynamic size and zeta potentials of the NPs were also measured at different pHs, and compared with dopamine-coated NPs. Stability of conjugated NPs in biological medium was tested as a function of incubation times. The variation in NP sizes and charges was mainly used to determine whether the

* Corresponding author.
E-mail address: ybao@eng.ua.edu (Y. Bao).

http://dx.doi.org/10.1016/j.jmmm.2016.10.039
Received 26 June 2016; Accepted 8 October 2016
Available online 13 October 2016
0304-8853/

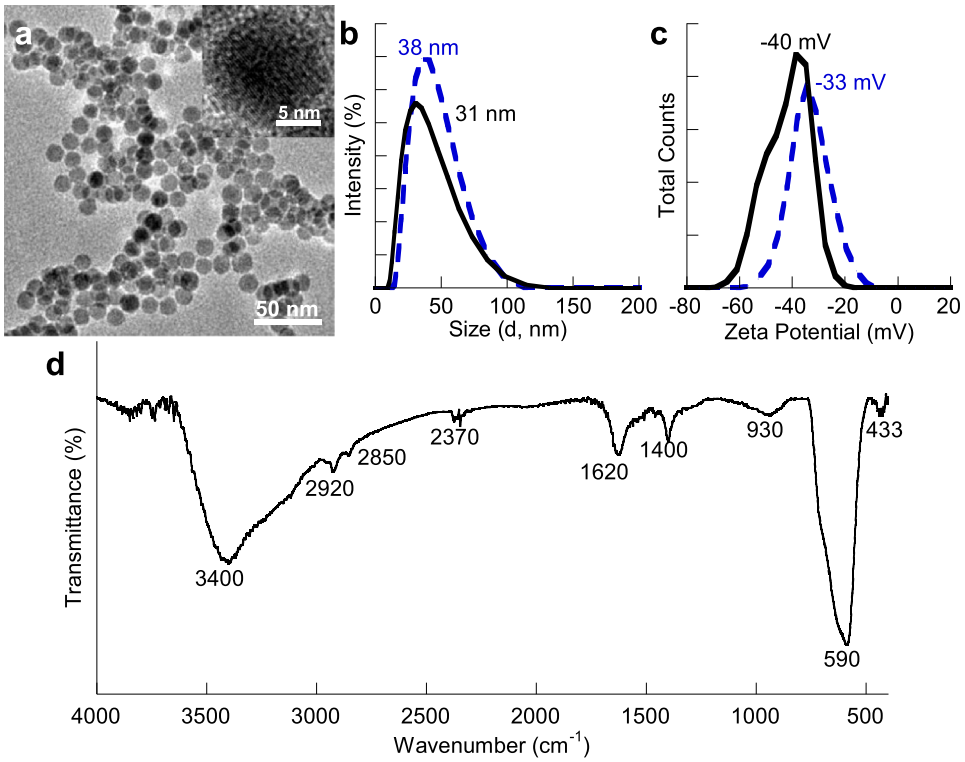

Fig. 1. Dopamine-coated NPs (a) TEM and high resolution images (insert), (b) DLS plots at pH 6 (dashed blue) and 9 (black), (c) zeta potential measurements pH 6 (dashed blue) and 9 (black), and (d) FTIR spectrum after activation. (For interpretation of the references to color in this figure legend, the reader is referred to the web version of this article.).

conjugated NPs affect surface protein adsorption. The study provides a general platform to link various small molecules onto iron oxide NPs, which provides a set of NPs for various biological and biomedical studies.

2. Experimental

2.1. Dopamine-coated nanoparticles

The spherical iron oxide NPs were synthesized *via* thermal decomposition following our previously established procedures [39]. Specifically, an iron oleate precursor was decomposed in the presence of oleic acid (OA) and trioctlphosphine oxide (TOPO) at 320 °C for 2.5 h. Subsequently, the hydrophobic ligands of NPs were replaced with dopamine molecules *via* a ligand exchange method with some modifications [36,37,39,40]. In brief, 1 mL of as-synthesized iron oxide NPs in chloroform (5 mg/mL) was mixed with 2 mL of dopamine aqueous solution (3 mg/mL). The mixture was sonicated for 5 min to form an emulsion, followed by the addition of 15 mL of acetone to facilitate phase transfer. The NPs were then separated out of solution *via* magnetic separation and washed three times with water to remove free dopamine. The dopamine-coated NPs were then dispersed in water to form a stock solution of (1 mg/mL). Before conjugation, the NP surfaces were activated with addition of NaOH, where the pH increase facilitates the formation of quinone structure from the catechol groups of dopamine. The quinone structure allows for facile conjugation of molecules containing $-NH_2$ or –SH groups *via* Schiff base or Michael's addition [38].

2.2. Conjugation of small molecules

Small molecule conjugation was achieved by simply mixing the activated NP solution with conjugation molecules at a 1:10 molar ratio based on the theoretical amount of dopamine on the NP surfaces. The use of excess small molecules allows for full coverage of NP surfaces with conjugating molecules. NP aqueous solution was degassed using Argon gas prior to the conjugation to prevent oxidation of some small molecules. In order to ensure maximum conjugation efficiency, NPs were activated immediately prior to conjugation with the addition of NaOH to adjust the pH to 9. The reaction mixture of activated NPs and small molecules were incubated at 37 °C for 12 h. After three washes with water, the conjugated NPs were collected for further analysis. NPs were characterized using transmission electron microscopy (TEM), dynamic light scattering (DLS), and Fourier transform infrared spectroscopy (FTIR) to verify the presence of the small molecules on the surface of the NPs.

The stability of the NPs was assessed by dispersing conjugated NPs in 10% fetal bovine serum (FBS) Eagle's minimal essential medium (EMEM) and incubated at 37 °C for up to 4 h. The 4 h incubation was chosen based on prior reports that 4 h incubation is required for *in vitro* cellular uptake [13,38]. DLS measurements (size and zeta potential) were performed at t=0, 30 min, 2 h, and 4 h to determine if the NPs experienced non-specific binding of serum proteins on the NPs surfaces.

3. Results and discussion

The iron oxide NPs were synthesized *via* thermal decomposition at high temperature in organic solvent, which produced monodisperse, highly crystalline NPs. Subsequently, the organic ligands were replaced with dopamine where a thin polydopamine layer likely formed, leaving the catechol groups on the NP surface for further conjugation. Fig. 1a shows the TEM image of 12 nm dopamine-coated iron oxide NPs from a typical reaction. The NPs were well dispersed after ligand exchange and retained their high crystallinity (Fig. 1, insert). The hydrodynamic size of the dopamine-coated NPs in solution at pH 6 from DLS was about 38 nm (Fig. 1b), which was much larger than the core size of 12 nm. The size increase was possibly resulted from either hydrogen bond formation between neighboring catechol groups or formation of a thin layer of polydopamine during the ligand exchange [37]. With

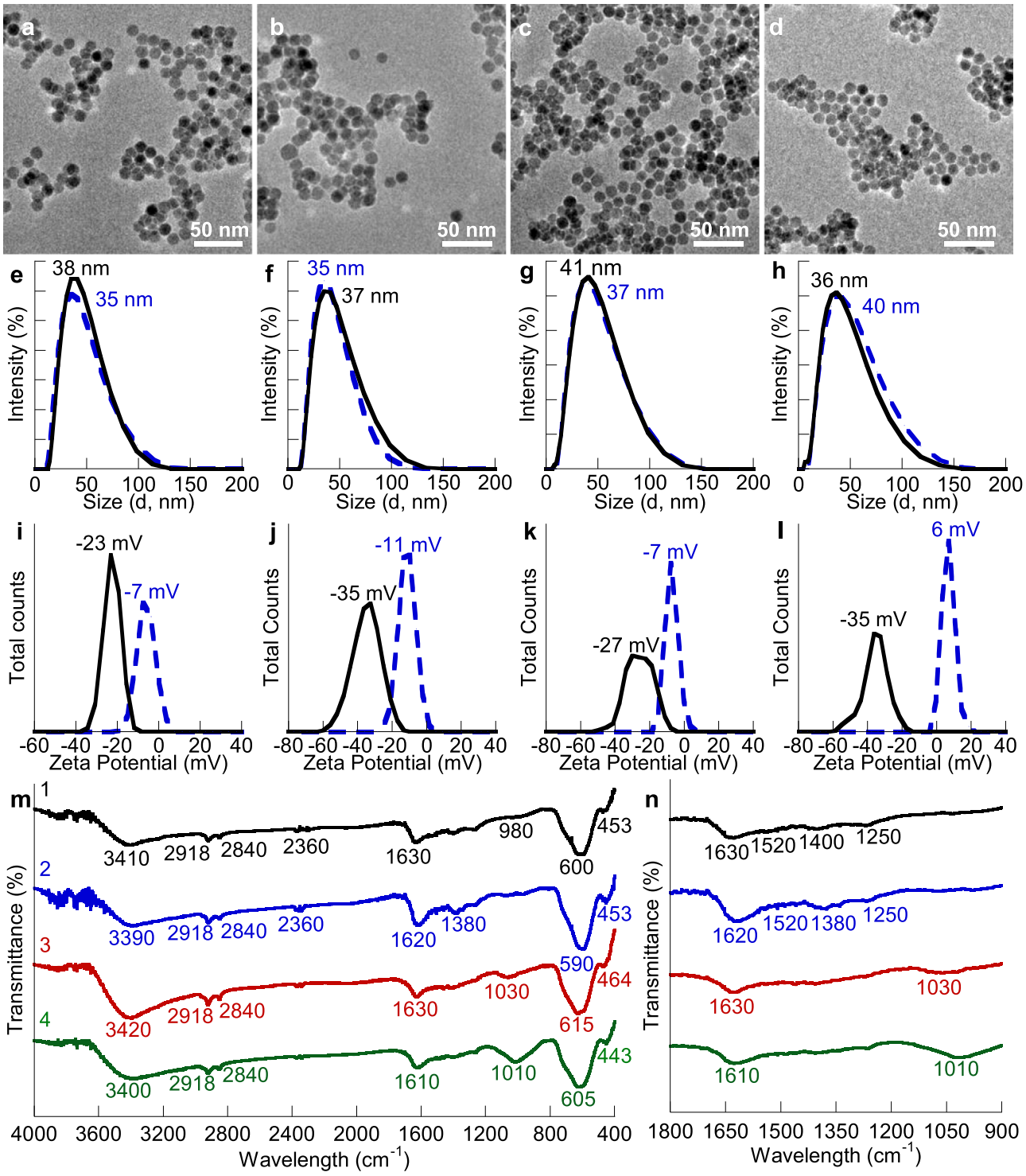

Fig. 2. Conjugated NPs with GSH (a, e, i, and m1), Cys (b, f, j, and m2), Lys(c, g, k, and m3), and Tris (d, h, l, and m4). (a–d) TEM images, (e–h) DLS plots pH 6 (dashed blue) and 9 (black), (i–l) zeta potential plots at pH 6 (dashed blue) and 9 (black), (m) FTIR spectra, and (n) detailed scan of FTIR spectra in the range of 900–1800 cm^{-1}. (For interpretation of the references to color in this figure legend, the reader is referred to the web version of this article.).

increasing solution pH to 9, the NP size decreased to 31 nm because of deprotonation of surface functional groups, which helped to further separate NPs from each other (Fig. 1b).

The dopamine-coated NPs were stable at pH 9 for long periods of time, but showed visible precipitation at pH below 6. The zeta potentials of these NPs at pH 6 and 9 were about was −33 mV and −40 mV respectively (Fig. 1c). The slightly lower zeta-potential at pH 9 is another indication of more deprotonation of catechol groups at higher pH. However, the absolute zeta-potential values of these NPs at pH 6 and 9 were both above 30, an indication of NP stability in solution. Fig. 1d shows the FTIR spectra of dopamine-coated NPs after activation. The detailed analysis of the dopamine-coated NPs before and after surface activation was reported previously by our group [41]. In brief, the characteristic peak at 3400 cm^{-1} corresponded to the catechol of dopamine. The peaks for aromatic C=C bonds appeared around 1400 cm^{-1} with a strong –CH=CH– ring breathing mode around 930 cm^{-1}. The characteristic –C=O band in Quinone structure at 1620 cm^{-1} was an indication of successful activation of dopamine

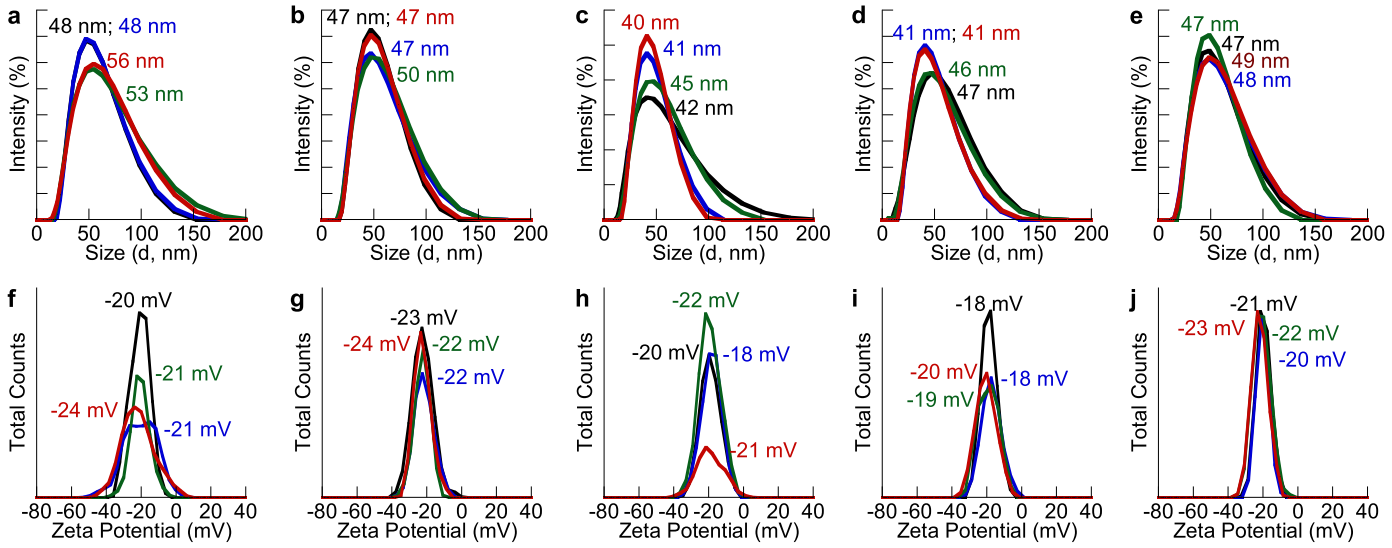

Fig. 3. DLS and zeta-potential plots of dopamine-coated NPs (a and f), conjugation with GSH (b and g), Cys (c and h), Lys (d and i) and Tris (e and j) in 10% FBS supplemented medium incubation time t=0 (black), 30 min (blue), 2 h (green), and 4 h (red). (For interpretation of the references to color in this figure legend, the reader is referred to the web version of this article.).

molecules on NP surfaces. The lack of the typical phenol alcohol band at 1065 cm^{-1} was another indication of successful activation. The absorption bands at lower wavenumbers (590 and 433 cm^{-1}) were related to Fe–O bonds in the tetrahedral and octahedral sites. The tetrahedral sites have a lower bond length with expected higher stretching frequency, where the 590 cm^{-1} corresponds to the intrinsic stretching vibrations of the Fe-O at the tetrahedral sites. The octahedral Fe-O stretching is normally around 400 cm^{-1} with a much weaker intensity [42].

After conjugated with various small molecules, the size and size distribution of NPs were not affected (Fig. 2a–d). In addition, the conjugated NPs were well dispersed without evident aggregations. Because of the small sizes of conjugating molecules, the hydrodynamic sizes of NPs did not show significant variations (Fig. 2e–h). However, the zeta-potential of the NPs was altered greatly after conjugation (Fig. 2i–l). Compared to the zeta-potentials of −33 mV and −40 mV at pH 6 and 9 for dopamine-coated NPs, the zeta-potentials of conjugated NPs at pH 6 and 9 were −7 and −23 mV for GSH conjugation, −11 and −35 mV for Cys conjugation, −7 and −27 mV for Lys conjugation, and 6 and −35 mV for Tris conjugation. The changes in zeta-potentials was an indication of successful conjugation. Because the activated dopamine molecules interact with amine and thiol groups, the conjugation of GSH, Cys, and Lys generated zwitterionic forms, where the surface charges change with pH. In contrast, the conjugation of Tris, generated close to neutral surface at pH of 6 and more negatively charged surface at pH 9.

The conjugation of GSH, Cys, Lys, and Tris onto dopamine-coated NP surfaces were evaluated with FTIR as shown in Fig. 2m. Fig. 2n is the detailed scan in the range of 900–1800 cm^{-1}. The broad peak around 3400 cm^{-1} in the FTIR spectra is the characteristic –OH stretching in alcohols and phenols, such as 3410 cm^{-1} for GSH (m1), 3390 cm^{-1} for Cys (m2), 3420 cm^{-1} for Lys (m3), and 3400 cm^{-1} for Tris (m4) respectively. Additionally, all 4 FTIR spectra showed the disappearance of the characteristic aromatic –C=C– peaks (1400 cm^{-1}) and the disappearance of the strong –CH=CH– ring breathing mode (930 cm^{-1}), both of which were a strong presence in the FTIR of the activated dopamine coated NPs. The small, sharp but weak peaks for both GSH and Cys around 2400 cm^{-1} can be assigned to thiol groups, because both of them contain thiol groups with characteristic peaks from 2550 to 2600 cm^{-1}. The disappearance and downward shift of those peaks to 2400 cm^{-1} indicated thiol attachment to dopamine-coated NPs. The detailed scan in the range of 900–1800 cm^{-1} showed characteristic NH_2-scissoring around 1500 cm^{-1}, which were not observed in the dopamine coated NPs (Figure 2n). The weak broad peaks at 1250 cm^{-1} were likely from the –C–O–C asymmetric stretching.

In contrast, the FTIR spectra of Lys and Tris showed no evident peaks in the 1500 cm^{-1} range indicating the attachment of amine groups onto NP surfaces. FTIR spectrum for Tris was similar to spectrum of dopamine-coated NPs, but without the aromatic C=C peaks. The appearance of the characteristic C–O stretching (for –OH) at 1010 cm^{-1} also suggested Tris attachment. FTIR spectrum for Lys conjugated NPs exhibited strong peaks at 2918 and 2840 cm^{-1} compared to other conjugations. These peaks were characteristic –C–C– stretching, arising from the long C–C side chain of Lys.

The non-specific serum protein adsorption of conjugated NPs was studied in EMEM medium at physiological pH and compared with dopamine-coated NPs. The DLS plots of NPs were measured at incubation time of 0, 30 min, 2 h and 4 h (Fig. 3). Dopamine-coated NPs showed an initial size increase from 31 to 48 nm and a significant drop in surface charge from −40 to −20 mV. After 4 h incubation, the hydrodynamic size of dopamine-coated NPs increased to 56 nm with an overall size increase of 25 nm. GSH-conjugated NPs showed an initial increase in size of about 10 nm and maintained this size throughout the entire 4 h. Cys-conjugated NPs experienced an initial size increase of 5 nm. Interestingly, NPs had a reduction of size with a narrower size distribution with increasing incubation time. Only 3 nm size increase was observed after 4 h incubation. Lys-conjugated NPs displayed an initial size increase of 6 nm. Similar to the Cys-conjugated NPs, a decrease in size with narrower size distribution was observed with respect to incubation time. Tris-conjugated NPs exhibited an initial size increase of 11 nm and maintained that size throughout the 4 h study. For all of the conjugated NPs, the zeta potentials were close to neutral. It was difficult to differentiate whether surface charge change resulted from protein absorption or pH effects, because the pH had a major effect on the charge of the conjugated NPs at different pHs. The hydrodynamic sizes of conjugated NPs all showed an initial size increase, but without significant variation with increasing incubation time, likely because of the Zwitterionic or neutral surfaces. The proteins may have initially bound to the surfaces, but once the net charge of the ligands became neutral, additional protein absorption was prevented. In contrast, dopamine-coated NPs showed a large increase in size and drop in zeta potential. Therefore, we believe that the conjugated NPs exhibited increased stability in physiological

conditions compared to dopamine-coated NPs, which could potentially reduce non-specific protein adsorption on the NPs surfaces and potentially increase *in vivo* circulation time.

4. Conclusion

In summary, we have demonstrated effective conjugation of four amine/ thiol containing small molecules onto dopamine-coated iron oxide NP surfaces *via* Schiff base or Michael's addition. By attaching either GSH, Cys, Lys, or Tris to NP surfaces, different surface functionalities were achieved as confirmed by FTIR spectra. In addition, the surface charges of NPs can be adjusted with pH depending on the surface coatings. Importantly, the surface conjugation resulted either Zwitterionic or neutral surfaces, which increase the NP stability in solution and minimized absorption of serum proteins in cell. Therefore, the conjugation can potentially increase *in vivo* circulation time due to reduced immune response. This facile conjugation method opens up possibilities for attaching various surface functionalities onto iron oxide NP surfaces for biomedical applications.

Acknowledgements

This work was supported in part by U.S. National Science Foundation (DMR1149931). We acknowledge the UA Central Analytical Facility (CAF) and the Biological Science Department for the use of TEM.

References

[1] X.-H. Peng, X. Qian, H. Mao, A.Y. Wang, Z.G. Chen, S. Nie, D.M. Shin, Targeted magnetic iron oxide nanoparticles for tumor imaging and therapy, Int. J. Nanomed. 3 (2008) 311–321.
[2] J.W.M. Bulte, T. Douglas, B. Witwer, S.-C. Zhang, E. Strable, B.K. Lewis, H. Zywicke, B. Miller, P. van Gelderen, B.M. Moskowitz, I.D. Duncan, J.A. Frank, Magnetodendrimers allow endosomal magnetic labeling and in vivo tracking of stem cells, Nat. Biotechnol. (2001) 1141–1147.
[3] J.V. Frangioni, R.J. Hajjar, In vivo tracking of stem cells for clinical trials in cardiovascular disease, Circulation (2014) 3378–3383.
[4] A. Taylor, A. Herrmann, D. Moss, V. Sée, K. Davies, S.R. Williams, P. Murray, Assessing the efficacy of nano- and micro-sized magnetic particles as contrast agents for MRI cell tracking, PLoS One 9 (2014) e100259.
[5] R. Weissleder, M. Nahrendorf, M.J. Pittet, Imaging macrophages with nanoparticles, Nat. Mater. 13 (2014) 125–138.
[6] B.J. McCullough, O. Kolokythas, J.H. Maki, D.E. Green, Ferumoxytol in clinical practice: implications for MRI, J. Magn. Reson. Imaging (2013) 1476–1479.
[7] P. Reimer, T. Balzer, Ferucarbotran (Resovist): a new clinically approved RES-specific contrast agent for contrast-enhanced MRI of the liver: properties, clinical development, and applications, Eur. Radiol. 13 (2003) 1266–1276.
[8] H. Shokrollahi, Contrast agents for MRI, Mater. Sci. Eng. 33 (2013) 4485–4497.
[9] G.J. Strijkers, W.J.M. Mulder, G.A.F. van Tilborg, K. Nicolay, MRI contrast agents: current status and future perspectives, anti-cancer agents in medical chemistry 7 (2007).
[10] M.J.D. Clift, B. Rothen-Rutishauser, D.M. Brown, R. Duffin, K. Donaldson, L. Proudfoot, K. Guy, V. Stone, The impact of different nanoparticle surface chemistry and size on uptake and toxicity in a murine macrophage cell line, Toxicol. Appl. Pharmacol. 232 (2008) 418–427.
[11] C. Chouly, D. Pouliquen, I. Lucet, J.J. Jeune, P. Jallet, Development of super-paramagnetic nanoparticles for MRI: effect of particle size, charge and surface nature on biodistribution, J. Microencapsul. 13 (1996) 245–255.
[12] S.M. Moghimi, A.C. Hunter, J.C. Murray, Long-circulating and target-specific nanoparticles: theory to practice, Pharmacol. Rev. 53 (2001) 283–318.
[13] Y. Xu, J.A. Sherwood, K.H. Lackey, Y. Qin, Y. Bao, The responses of immune cells to iron oxide nanoparticles, J. Appl. Toxicol. 36 (2016) 543–553.
[14] O. Lunov, T. Syrovets, C. Rocker, K. Tron, G.U. Nienhaus, V. Rasche, V. Mailander, K. Landfester, T. Simmet, Lysosomal degradation of the carboxydextran shell of coated superparamagnetic iron oxide nanoparticles and the fate of professional phagocytes, Biomaterials 31 (2010) 9015–9022.
[15] M.P. Monopoli, C. Aberg, A. Salvati, K.A. Dawson, Biomolecular coronas provide the biological identity of nanosized materials, Nat. Nanotechnol. 7 (2012) 779–786.
[16] M. Lundqvist, J. Stigler, G. Elia, I. Lynch, T. Cedervall, K.A. Dawson, Nanoparticle size and surface properties determine the protein corona with possible implications for biological impacts, Proc. Natl. Acad. Sci. USA 105 (2008) 14265–14270.
[17] E. Poselt, H. Kloust, U. Tromsdorf, M. Janschel, C. Hahn, C. Maßlo, H. Weller, Relaxivity optimization of a pegylated iron-oxide-based negative magnetic resonance contrast agent for T_2, ACS Nano (2012) 1619–1624.
[18] K.P. García, K. Zarschler, L. Barbaro, J.A. Barreto, W. O'Malley, L. Spiccia, H. Stephan, B. Graham, Zwitterionic-coated stealth nanoparticles for biomedical applications: recentrecent advances in countering biomolecular corona formation and uptake by the mononuclear phagocyte system, Small 10 (2014) 2516–2529.
[19] D.-F. Liu, C. Qian, Y.-L. An, D. Chang, S.-H. Ju, G.-J. Teng, Magnetic resonance imaging of post-ischemic blood-brain barrier damage with PEGylated iron oxide nanoparticles, Nanoscale 6 (2014) 15161–15167.
[20] H. Wei, N. Insin, J. Lee, H.-S. Han, J.M. Cordero, W. Liu, M.G. Bawendi, Compact zwitterion-coated iron oxide nanoparticles for biological applications, Nano Lett. 12 (2012) 22–25.
[21] R.A. Sperling, W.J. Parak, Surface modification, functionalization and bioconjugation of colloidal inorganic nanoparticles, Philos. Trans. R. Soc. Lond. A-Math. Phys. Eng. Sci. 368 (2010) 1333–1383.
[22] C.G. Hadjipanayis, R. Machaidze, M. Kaluzova, L.Y. Wang, A.J. Schuette, H.W. Chen, X.Y. Wu, H. Mao, EGFRvIII antibody-conjugated iron oxide nanoparticles for magnetic resonance imaging-guided convection-enhanced delivery and targeted therapy of glioblastoma, Cancer Res. 70 (2010) 6303–6312.
[23] M. Mahmoudi, A. Simchi, M. Imani, Recent advances in surface engineering of superparamagnetic iron oxide nanoparticles for biomedical applications, J. Iran. Chem. Soc. 7 (2010) S1–S27.
[24] J. Nam, N. Won, J. Bang, H. Jin, J. Park, S. Jung, Y. Park, S. Kim, Surface engineering of inorganic nanoparticles for imaging and therapy, Adv. Drug Deliv. Rev. 65 (2013) 622–648.
[25] N. Erathodiyil, J.Y. Ying, Functionalization of inorganic nanoparticles for bioimaging applications, Acc. Chem. Res. 44 (2011) 925–935.
[26] J.M. Montenegro, V. Grazu, A. Sukhanova, S. Agarwal, J.M. de la Fuente, I. Nabiev, A. Greiner, W.J. Parak, Controlled antibody/(bio-) conjugation of inorganic nanoparticles for targeted delivery, Adv. Drug Deliv. Rev. 65 (2013) 677–688.
[27] W. Wei, Q.G. He, C. Hong, Surface functionalization and application for magnetic iron oxide nanoparticles, Prog. Chem. 20 (2008) 265–272.
[28] D. Arndt, T.M. Gesing, M. Baeumer, Surface functionalization of iron oxide nanoparticles and their stability in different media, Chempluschem 77 (2012) 576–583.
[29] J. Kalia, R.T. Raines, Advances in bioconjugation, Curr. Org. Chem. 14 (2010) 138–147.
[30] G.T. Hermanson, Bioconjugate Techniques, 2nd ed., Academic Press, Rockford, Illinois, USA, 2008.
[31] C.W. Lee, K.T. Huang, P.K. Wei, Y.D. Yao, Conjugation of γ-Fe2O3 nanoparticles with single strand oligonucleotides, J. Magn. Magn. Mater. 304 (2006) e412–e414.
[32] F. Shamsipour, A.H. Zarnani, R. Ghods, M. Chamankhah, F. Forouzesh, S. Vafaei, A.A. Bayat, M.M. Akhondi, M. Ali Oghabian, M. Jeddi-Tehrani, Conjugation of monoclonal antibodies to super paramagnetic iron oxide nanoparticles for detection of her2/neu antigen on breast cancer cell lines, Avicenna J. Med. Biotechnol. 1 (2009) 27–31.
[33] R.A. Sperling, W.J. Parak, Surface modification, functionalization and bioconjugation of colloidal inorganic nanoparticles, Philos. Trans. R. Soc. Lond. A: Math. Phys. Eng. Sci. 368 (2010) 1333–1383.
[34] L. Maurizi, H. Bisht, F. Bouyer, N. Millot, Easy route to functionalize iron oxide nanoparticles via long-term stable thiol groups, Langmuir 25 (2009) 8857–8859.
[35] M. Mazur, A. Barras, V. Kuncser, A. Galatanu, V. Zaitzev, K.V. Turcheniuk, P. Woisel, J. Lyskawa, W. Laure, A. Siriwardena, R. Boukherroub, S. Szunerits, Iron oxide magnetic nanoparticles with versatile surface functions based on dopamine anchors, Nanoscale 5 (2013) 2692–2702.
[36] Y.L. Xu, S. Palchoudhury, Y. Qin, T. Macher, Y.P. Bao, Make conjugation simple: aa facile approach to integrated nanostructures, Langmuir 28 (2012) 8767–8772.
[37] Y.L. Xu, D.C. Baiu, J.A. Sherwood, M.R. McElreath, Y. Qin, K.H. Lackey, M. Otto, Y.P. Bao, Linker-free conjugation and specific cell targeting of antibody functionalized iron-oxide nanoparticles, J. Mater. Chem. B 2 (2014) 6198–6206.
[38] Y. Xu, D.C. Baiu, J.A. Sherwood, M.R. McElreath, Y. Qin, K.H. Lackey, M. Otto, Y. Bao, Linker-free conjugation and specific cell targeting of antibody functionalized iron-oxide nanoparticles, J. Mater. Chem. B 2 (2014) 6198–6206.
[39] Y.L. Xu, Y. Qin, S. Palchoudhury, Y.P. Bao, Water-soluble iron oxide nanoparticles with high stability and selective surface functionality, Langmuir 27 (2011) 8990–8997.
[40] A. Riedinger, P. Guardia, A. Curcio, M.A. Garcia, R. Cingolani, L. Manna, T. Pellegrino, Subnanometer local temperature probing and remotely controlled drug release based on azo-functionalized iron oxide nanoparticles, Nano Lett. 13 (2013) 2399–2406.
[41] Y. Xu, S. Palchoudhury, Y. Qin, T. Macher, Y. Bao, Make conjugation simple: a facile approach to integrated nanostructures, Langmuir 28 (2012) 8767–8772.
[42] Y. Xu, J. Sherwood, Y. Qin, R.A. Holler, Y. Bao, A general approach to the synthesis and detailed characterization of magnetic ferrite nanocubes, Nanoscale 7 (2015) 12641–12649.